



Contents lists available at ScienceDirect

# Journal of Quantitative Spectroscopy & Radiative Transfer

journal homepage: [www.elsevier.com/locate/jqsrt](http://www.elsevier.com/locate/jqsrt)

## Radar polarimetry of Saturn's rings: Modeling ring particles as fractal aggregates built of small ice monomers

Michael I. Mishchenko<sup>a,\*</sup>, Janna M. Dlugach<sup>b</sup><sup>a</sup> NASA Goddard Institute for Space Studies, 2880 Broadway, New York, NY 10025, USA<sup>b</sup> Main Astronomical Observatory of the National Academy of Sciences of Ukraine, 27 Zabolotny Str., 03680 Kyiv, Ukraine

### ARTICLE INFO

#### Article history:

Received 20 November 2008

Received in revised form

26 December 2008

Accepted 21 January 2009

#### Keywords:

Polarimetry

Multiple scattering

Radiative transfer

Coherent backscattering

Remote sensing

Radar

Saturn's rings

### ABSTRACT

We analyze ground-based radar polarimetric observations of Saturn's rings at a wavelength of 12.6 cm by employing the model of a vertically and horizontally plane-parallel homogeneous slab composed of clumpy particles in the form of fractal aggregates of small ice monomers. Our model takes full account of the effects of polarization, multiple scattering, and coherent backscattering. Using efficient superposition *T*-matrix and vector radiative transfer codes, we perform computations of the backscattering circular polarization ratio for fractal aggregates generated with a cluster–cluster aggregation model and having the following characteristics: monomer refractive index  $m = 1.78 + i0.003$ ; monomer packing density  $p = 0.2$ ; fractal dimensions  $D_f = 2.5$  and 3; and overall fractal radii  $R$  in the range  $4 \leq R \leq 10$  cm. In order to obtain physically realistic values of single-scattering properties of the aggregates we perform averaging over an ensemble of clusters generated for the same values of fractal parameters but having different geometrical configurations of the monomers. We conclude that in the framework of the above morphological model of Saturn's rings and the specific cluster–cluster aggregation procedure, it may be problematic to obtain a satisfactory and realistic agreement between theoretical computations and the observed values of the radar circular polarization ratio.

Published by Elsevier Ltd.

### 1. Introduction

In this paper we extend the analysis of the radar measurements of the backscattering circular polarization ratio for the A and B rings of Saturn performed at a wavelength of 12.6 cm [1,2]. In our recent study [3], we employed the model of the rings in the form of a vertically and horizontally homogeneous particulate slab and fully accounted for the effects of polarization, multiple scattering, and weak localization (otherwise known as coherent backscattering) as well as of nonsphericity of the ring particles. Ring particle shapes were parameterized using the models of randomly oriented Chebyshev particles, oblate or prolate spheroids with a fixed aspect ratio, and an equiprobable shape mixture of oblate and prolate spheroids. Our computations have demonstrated that it is impossible to reproduce the observational data without an explicit inclusion of the effect of coherent backscattering. Also our model simulations favored the model of ring bodies in the form of nearly spherical ice particles with small-scale surface roughness and an effective radius in the range 4–10 cm. The ring vertical optical thickness (within the wakes) was estimated to be in the range of 2–3 or even larger.

It is not inconceivable, however, that the ring particles have more complex morphologies than those analyzed in [3]. Therefore, the next step in our analysis of the results of radar polarization observations documented in [1,2] is to

\* Corresponding author. Tel.: +1 212 678 5590; fax: +1 212 678 5622.

E-mail address: [mmishchenko@giss.nasa.gov](mailto:mmishchenko@giss.nasa.gov) (M.I. Mishchenko).

investigate the case of ring particles in the form of aggregates composed of densely packed ice monomers. As an initial model of such aggregates we adopt fractal clusters composed of monodisperse ice spheres. It was shown in [4] that such aggregates can be described by the following statistical scaling law:

$$N_S = k_0 \left( \frac{R_g}{r} \right)^{D_f}, \quad (1)$$

where  $r$  is the monomer radius,  $1 \leq D_f \leq 3$  is the fractal dimension,  $k_0$  is the fractal prefactor,  $N_S$  is the number of monomers in the aggregate, and  $R_g$ , called the radius of gyration, is a measure of the overall aggregate radius. Both  $D_f$  and  $k_0$  specify the morphology of a fractal aggregate. Densely packed aggregates have  $D_f$  values close to 3, whereas the fractal dimension of chain-like and branched clusters can be much smaller. The prefactor  $k_0$  is also related to the compactness state of a fractal such that, for a fixed  $D_f$ , the packing density tends to be smaller as  $k_0$  decreases (see, e.g., [5]).

Consistent with the above rationale, the purpose of this sequel paper is to present and discuss the results of computations of the radar circular polarization ratio for the model of Saturn's rings in the form of a plane-parallel random particulate medium composed of ice fractal aggregates described by Eq. (1).

## 2. Computational approach

Consistent with [3], the numerical modeling of the radar circular polarization ratio for Saturn's rings involves the following steps:

1. the computation of the requisite single-scattering properties of the aggregate ring particles,
2. the computation of the diffuse Stokes reflection matrix through the explicit numerical solution of the vector radiative transfer equation (VRTE),
3. the computation of the requisite characteristics of coherent backscattering from the diffuse Stokes reflection matrix and
4. the computation of the circular polarization ratio.

The procedure for the computation of the single-scattering characteristics of fractal-like ice clusters includes two steps. First, we use the cluster–cluster aggregation procedure developed by Mackowski [6] to generate monomer positions in a fractal aggregate. The basic idea of this method is to generate a sequence of random sphere positions subject to the constraint that the positions, at any point in the sequence, identically satisfy Eq. (1) for given  $k_0$  and  $D_f$  and that each monomer touches at least one other monomer. Then we apply the efficient superposition  $T$ -matrix method developed for multisphere clusters in random orientation [7]. The corresponding computer code is publicly available on-line [8], yields numerically exact results within the range of numerical convergence, and has been extensively used in a wide range of applications [9–11].

After the single-scattering characteristics of aggregate particles have been determined, they are used to compute the elements of the diffuse Stokes reflection matrix. To this end, we employ a vector radiative-transfer code based on the numerical solution of the Ambarzumian's nonlinear integral equation and applicable to a semi-infinite homogeneous particulate slab [12,13]. For a finite slab, we use a numerically exact computer code based on the invariant imbedding technique [13,14].

Then the requisite characteristics of coherent backscattering are derived from the diffuse Stokes reflection matrix according to Eqs. (14.3.21)–(14.3.25) of [13]. The final step is to obtain the circular polarization ratio from Eq. (14.5.15) of [13].

## 3. Numerical results

As stated above, we use the model of Saturn's rings in the form of a plane-parallel homogeneous slab composed of fractal ice aggregates with the refractive index  $m = m_R + im_I = 1.78 + i0.003$ . The latter corresponds to weakly contaminated water ice at a wavelength of 12.6 cm [15]. The monomer packing density in the cluster  $p$  is fixed at 0.2, thereby corresponding to moderately dense aggregates. To investigate the effect of the fractal dimension  $D_f$  on the radar circular polarization ratio, computations have been performed for two values:  $D_f = 2.5$  and 3. In most of our calculations discussed below, the monomer radius  $r$  is assumed to be fixed at 1 cm, while the overall cluster radius  $R$  is varied starting from 4 cm in steps of 1 cm. The number of spherical monomers  $N_S$  and the fractal prefactor  $k_0$  can then be found from the relations

$$N_S = p(R/r)^3, \quad (2)$$

$$N_S = k_0 \left( \frac{R-r}{r} \right)^{D_f}. \quad (3)$$

In Table 1 we list the values of  $N_S$  and  $k_0$  derived from Eqs. (2) and (3) for several values of the overall fractal radius in the range  $4 \leq R \leq 10$  cm and for  $D_f = 2.5$  and 3.

**Table 1**

Fractal parameter values used in model computations.

$R$ (cm)	4	5	6	7	8	9	10
$N_S$	13	25	43	69	102	146	200
$k_0$ ( $D_f = 2.5$ )	0.83	0.78	0.77	0.78	0.79	0.81	0.82
$k_0$ ( $D_f = 3$ )	0.48	0.39	0.34	0.32	0.30	–	–

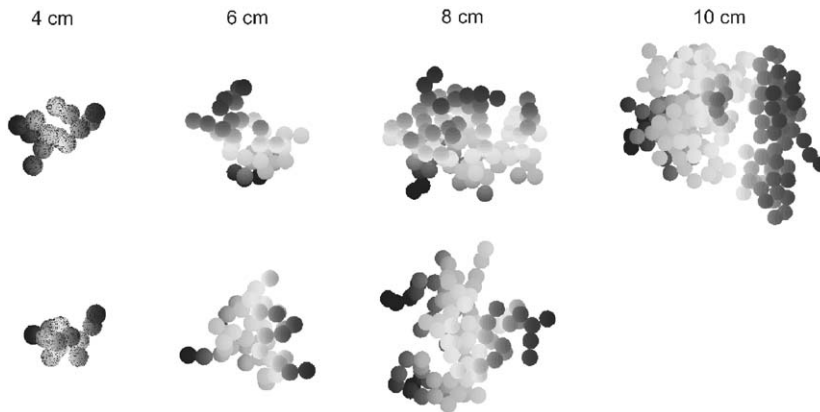
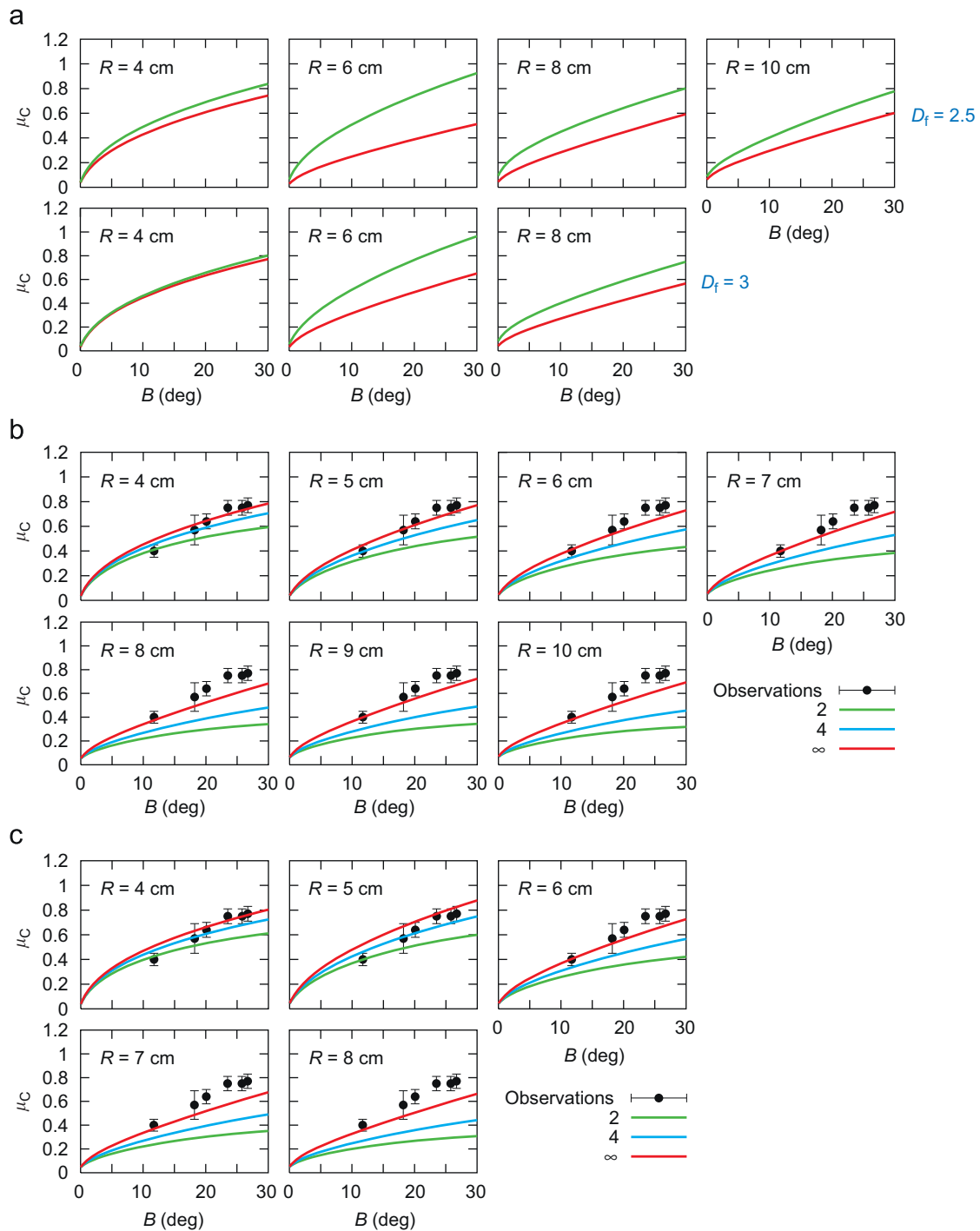
**Fig. 1.** Examples of clusters generated with the cluster–cluster procedure [6] for  $D_f = 2.5$  (top row) and 3 (bottom row),  $R = 4, 6, 8,$  and 10 cm, and the corresponding values of  $N_S$  and  $k_0$  listed in Table 1.

Fig. 1 shows examples of clusters generated by the cluster–cluster procedure described in [6] for  $D_f = 2.5$  and 3 and the values of  $N_S$  and  $k_0$  from Table 1. Interestingly, it appears that for the values of  $N_S$  and  $k_0$  determined from Eqs. (2) and (3) the cluster–cluster aggregation algorithm fails to perform for  $R > 10$  cm when  $D_f = 2.5$  and for  $R > 8$  cm when  $D_f = 3$ . We will see later, however, that this limitation does not necessarily affect the outcome of our study.

For each value of the overall radius  $R$  and the specified fractal parameters, we generate an ensemble of 10 fractal-parameter-equivalent realizations of an aggregate and then average the requisite single-scattering characteristics over the ensemble. This approach is motivated by the fact that each run of the cluster generation procedure results in a cluster with a different and unique geometrical configuration of the monomers. Therefore, a legitimate question is whether the scattering properties of a single fractal realization are sufficiently representative of all the clusters with the same fractal parameter values. The results for strongly absorbing soot fractals composed of a large number of small monomers ( $N_S = 400$ ) documented in [16] indicate that the scattering and absorption characteristics of only one cluster realization adequately represent the properties of the ensemble. On the other hand, the results for less absorbing particles demonstrate that in some cases averaging over a large set of fractal-parameter-equivalent clusters must be performed [17].

Fig. 2a illustrates the range of values of the backscattering circular polarization ratio  $\mu_C$  calculated for 10 fractal-parameter-equivalent cluster realizations as a function of the ring opening angle  $B$  (the angle between the line of sight and the ring plane). The computations are performed for a semi-infinite plane-parallel homogeneous layer composed of ice clusters with different values of  $R$  and the cluster parameter values listed in Table 1. One can see that the corresponding  $\mu_C$  values can vary by as much as 50% with cluster realization. For  $R = 4$  cm, the range of values is rather narrow, but then it increases with  $R$ , reaches a maximum, and then starts to decrease. We also see that with increasing  $D_f$  from 2.5 (the upper row of diagrams in panel 2a) to 3 (the lower row of diagrams) the range of variability decreases. Obviously, these results along with those of [16,17] suggest that it is highly desirable to perform in the future a detailed and comprehensive analysis of the effects of aggregate microphysical characteristics (such as the refractive index, number and size of monomers, and morphology) on the scattering and the absorption properties of an ensemble of fractal-parameter-equivalent clusters. The results shown in Fig. 2a do indicate that in order to compute physically relevant values of the radar circular polarization ratio, it is necessary to perform ensemble averaging.

Figs. 2b and c depict model dependences of the backscattering circular polarization ratio  $\mu_C$  on the ring opening angle  $B$  computed for  $D_f = 2.5$  and 3 and for various values of the ring optical thickness. Both figures also show the average measured values of  $\mu_C$  and the corresponding error bars [1,2]. We see that in all the cases considered, the model of the ring particles in the form of ice aggregates hardly allows one to obtain a realistic agreement between the results of the measurements and numerical simulations. For  $R \geq 6$  cm, even the model of optically semi-infinite rings yields values of the circular polarization ratio that are significantly smaller than the observed ones. The situation is somewhat better for  $R = 4$



**Fig. 2.** (a) Angular dependence of the maximal and minimal values of the radar circular polarization ratio for a semi-infinite particulate slab. The computations were performed for a range of cluster realizations with the same fractal parameters but different geometric configurations of the monomers. (b) Backscattering circular polarization ratio  $\mu_C$  versus ring opening angle  $B$  for a plane-parallel slab consisting of ice aggregates with the fractal dimension  $D_f = 2.5$ . Different colors correspond to different values of the ring optical thickness, as shown by the corresponding curve legends. (c) As in panel (b), but for the fractal dimension value  $D_f = 3$ .

and 5 cm and optical thicknesses  $\geq 4$ . Nevertheless, the theoretical fits are significantly worse than those rendered by Chebyshev particles, as discussed in [3], in that the range of acceptable fractal-radius values appears to be unrealistically narrow:  $3 \text{ cm} \leq R \leq 5 \text{ cm}$ . It is also interesting to note that there is no pronounced fractal-dimension dependence of  $\mu_C$  for the two values of  $D_f$  used in the computations.

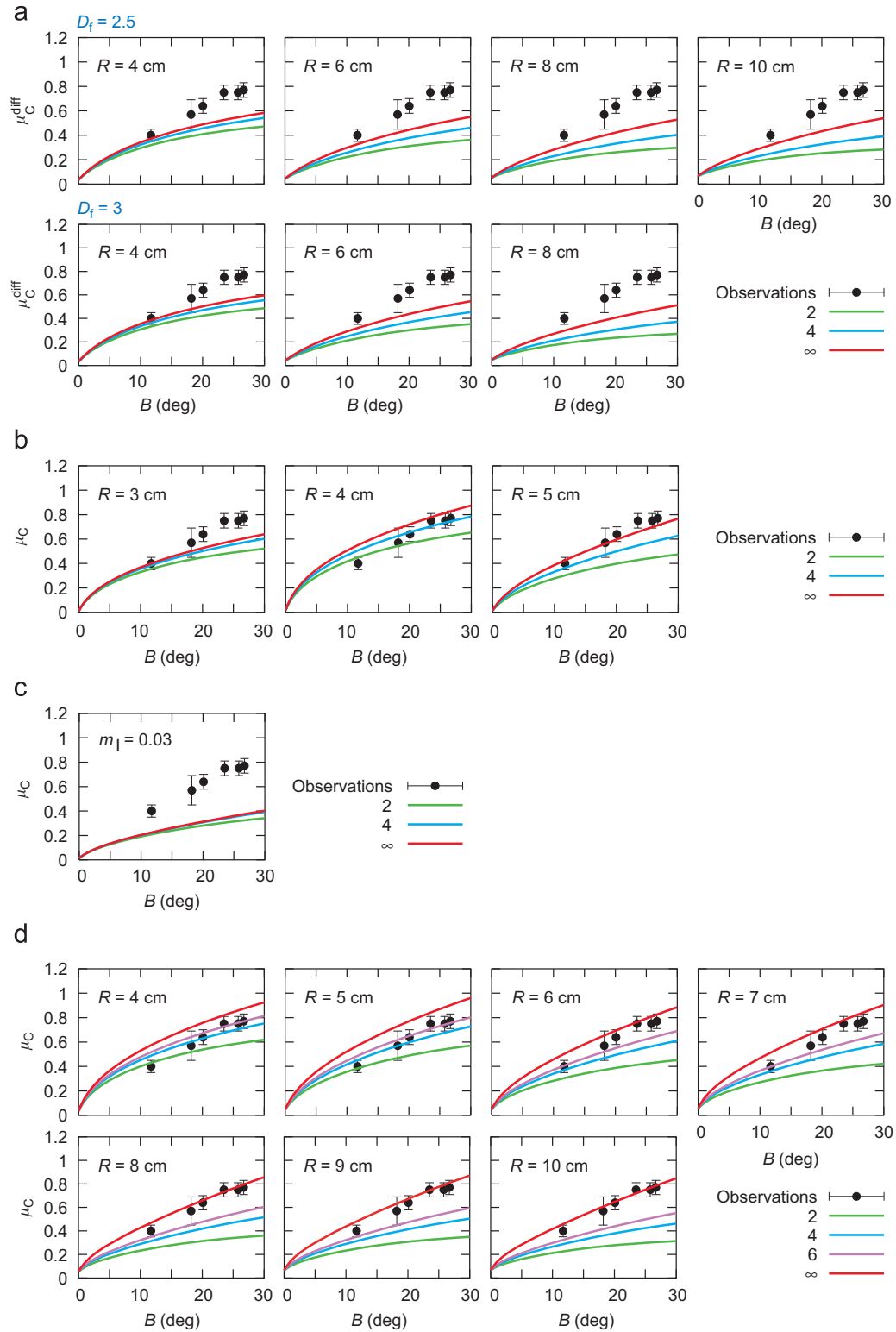


**Fig. 3.** (a) Angular dependence of the diffuse circular polarization ratio calculated by ignoring the effect of coherent backscattering. Different colors correspond to different values of the ring optical thickness, as shown by the corresponding curve legends. (b) As in Fig. 2b, but for the monomer radius 0.5 cm. (c) As in the right-hand diagram of panel (b), but for  $m_1 = 0.03$ . (d) As in Fig. 2b, but for  $m_1 = 0.0003$ .

#### 4. Discussion

The results of our analysis depend, of course, on the modeling strategy chosen. Our modeling approach can be called microphysical since it can be traced directly to the Maxwell equations [3,13,18]. The applicability of the VRTE does not impose specific limitations on the geometrical thickness of the rings, but does rely on the assumption of a low volume density of the scattering medium. Of course, it is not inconceivable that the particle volume density in the A and B rings of Saturn deviates from zero significantly. However, the results of [19] suggest that the theoretical predictions based on the VRTE should be valid for particle volume densities as high as 10%.

We have solved the VRTE assuming that the scattering medium is horizontally homogeneous, while it has been suggested recently (e.g., [20] and references therein) that Saturn's rings are likely to have a pronounced wake structure with particle density between the wakes dropping to almost zero. Nevertheless, our results should remain valid if the horizontal optical thickness of the individual wakes is significantly greater than their vertical optical thickness. Then the retrieved vertical optical thickness values should be attributed to an average wake rather than to the vertical optical thickness averaged over the entire horizontal extent of the rings. Indeed, recent studies do suggest that the individual wakes are geometrically thin [21] and can be modeled as broad, flat sheets of particles with relatively empty spaces between them [22,23]. This suggests that the plane-parallel particulate layer model used in this paper as well as in [3] should be adequate. Furthermore, while absolute measurements of the radar reflectance can indeed be affected by a pronounced wake structure, most 3D effects can be expected to cancel out in the computation of  $\mu_c$  upon dividing one radar reflectance by another.

An essential aspect of our model is the possibility to account explicitly for the effect of weak localization. Fig. 3a depicts the theoretical angular dependences of the diffuse circular polarization ratio obtained by neglecting the effect of coherent backscattering and using Eq. (14.5.16) of [13]. In agreement with our previous discussion in [3], the comparison of the model results shown in Figs. 2b and c with those in Fig. 3a clearly demonstrates that neglecting the contribution of coherent backscattering to  $\mu_c$  cannot improve the agreement of theoretical computations with measurement data.

Fig. 3b parallels Fig. 2b, but is computed for a monomer radius of  $r = 0.5$  cm. Again, it is obvious that decreasing the monomer radius does not result in a better fit. Of course, this result does not imply that particles with radii much smaller than  $\sim 1$  cm are not present in Saturn's rings. For example, an important constituent of the A and B rings are sub-micrometer ice grains which cause the famous photometric and polarimetric opposition effects when they form the regolith covering the larger ring bodies [24–29] and cause the spokes when they get levitated [30,31]. The existence of larger regolithic grains, with radii  $\sim 5$ – $20$   $\mu\text{m}$ , follows from analyses of spectroscopic observations [32]. However, such particles become Rayleigh scatterers with a negligibly small optical thickness at the wavelength 12.6 cm and are completely invisible to the radar. This explains our modeling choice of ice fractal monomers with radii  $\sim 1$  cm.

Another important modeling issue is the actual absorptivity of ice at the radar wavelength. There have been indications that although water ice is the dominant component of the ring particles, it likely contains impurities lowering the albedo of the rings at visible wavelengths [32–34]. The effect of such impurities on the imaginary part of the refractive index at 12.6 cm is unknown, but is likely to increase  $m_1$  with respect to the value 0.0001 typical of pure water ice [15]. All computations discussed above are based on the value  $m_1 = 0.003$ . Fig. 3c shows that a further increase of  $m_1$  is likely to result in a much worse fit, apparently owing to a significant decrease in the single-scattering albedo of the fractal aggregates and thus in a much reduced multiple-scattering contribution (including that due to weak localization) to  $\mu_c$ . On the other hand, the results shown in Fig. 3d indicate that using a much smaller value  $m_1 = 0.0003$ , which is more typical of uncontaminated water ice, results in a somewhat improved fit. However, the requisite optical thickness of the rings still appears to be unrealistically large. Such a variability of  $\mu_c$  with  $m_1$  is not typical of solid nonspherical ice particles studied in [3]. Obviously, the effect of  $m_1$  on  $\mu_c$  as a function of particle morphology deserves a further analysis.

#### 5. Conclusions

The results of our computations of the backscattering circular polarization ratio demonstrate that to obtain physically relevant values of the scattering properties of aggregate particles it is necessary to perform averaging over a variety of aggregates generated for the same values of the fractal parameters but having different internal arrangements of monomers. Unlike our previous results [3] obtained for nearly spherical ice particles with small-scale surface roughness, in the case of ice fractals we could not obtain a physically satisfactory agreement between the observed values of the radar circular polarization ratio [1,2] and the results of computations, except, perhaps, for an unrealistically narrow range of fractal radii around  $\sim 5$  cm and very large optical thickness values. Thus our study shows that the model of ring particles in the form of ice fractals generated by the cluster–cluster aggregation algorithm proposed in [6] is hardly consistent with the results of radar polarimetry of Saturn's rings [1,2]. We expect this conclusion to have important ramifications for the modeling of the formation and dynamical evolution of Saturn's rings [20,35,36].

It is worth remembering, however, that our analysis is explicitly based on the assumption that the average radar circular polarization ratios measured for the A and B rings of Saturn and reported in [1,2] are accurate and mutually consistent. This means that our conclusions may need to be revised should new and more reliable measurements show a significantly

different dependence of  $\mu_c$  on the ring opening angle. Furthermore, alternative cluster generation models should be thoroughly examined.

## Acknowledgments

We thank Dan Mackowski for providing his code for the computer generation of fractal clusters, Li Liu for help with computations, and an anonymous referee for useful comments. This research was supported by the NASA Radiation Sciences Program managed by Hal Maring.

## References

- [1] Ostro SJ, Pettengill GH, Campbell DB. Radar observations of Saturn's rings at intermediate tilt angles. *Icarus* 1980;41:381–8.
- [2] Nicholson PD, French RG, Campbell DB, et al. Radar imaging of Saturn's rings. *Icarus* 2005;177:32–62.
- [3] Mishchenko MI, Dlugach JM. Weak localization of electromagnetic waves and radar polarimetry of Saturn's rings. *Mon Not R Astron Soc* 2008;389:1665–74.
- [4] Sorensen CM. Light scattering by fractal aggregates: a review. *Aerosol Sci Technol* 2001;35:648–87.
- [5] Liu L, Mishchenko MI. Effects of aggregation on scattering and radiative properties of soot aerosols. *J Geophys Res* 2005;110:D11211.
- [6] Mackowski DW. A simplified model to predict the effects of aggregation on the absorption properties of soot particles. *JQSRT* 2006;100:237–49.
- [7] Mackowski DW, Mishchenko MI. Calculation of the  $T$ -matrix and the scattering matrix for ensembles of spheres. *J Opt Soc Am A* 1996;13:2266–78.
- [8] Mackowski DW. <ftp://ftp.eng.auburn.edu/pub/dmckowski/scatcodes/index.html>.
- [9] Mishchenko MI, Videen G, Babenko VA, et al.  $T$ -matrix theory of electromagnetic scattering by particles and its applications: a comprehensive reference database. *JQSRT* 2004;88:357–406.
- [10] Mishchenko MI, Videen G, Babenko VA, et al. Comprehensive  $T$ -matrix reference database: a 2004–06 update. *JQSRT* 2007;106:304–24.
- [11] Mishchenko MI, Videen G, Babenko VA, et al. Comprehensive  $T$ -matrix reference database: a 2006–07 update. *JQSRT* 2008;109:1447–60.
- [12] de Rooij WA. Reflection and transmission of polarized light by planetary atmospheres. PhD dissertation, Vrije Universiteit, Amsterdam; 1985.
- [13] Mishchenko MI, Travis LD, Lacis AA. Multiple scattering of light by particles: radiative transfer and coherent backscattering. Cambridge: Cambridge University Press; 2006.
- [14] Mishchenko MI. The fast invariant imbedding method for polarized light: computational aspects and numerical results for Rayleigh scattering. *JQSRT* 1990;43:163–71.
- [15] Warren SG, Brandt RE. Optical constants of ice from the ultraviolet to the microwave: a revised compilation. *J Geophys Res* 2008;113:D14220.
- [16] Liu L, Mishchenko MI. Scattering and radiative properties of complex soot and soot-containing aggregate particles. *JQSRT* 2007;106:262–73.
- [17] Kolokolova L, Kimura H, Ziegler K, Mann I. Light-scattering properties of random-oriented aggregates: do they represent the properties of an ensemble of aggregates. *JQSRT* 2006;100:199–206.
- [18] Mishchenko MI. Multiple scattering, radiative transfer, and weak localization in discrete random media: unified microphysical approach. *Rev Geophys* 2008;46:RG2003.
- [19] Mishchenko MI. Polarization effects in weak localization of light: calculation of the copolarized and depolarized backscattering enhancement factors. *Phys Rev B* 1991;44:12597–600.
- [20] Porco CC, Weiss JW, Richardson DC, Dones L, Quinn T, Throop H. Simulations of the dynamical and light-scattering behavior of Saturn's rings and the derivation of ring particle and disk properties. *Astron J* 2008;136:2172–200.
- [21] Hedman MM, Nicholson PD, Salo H, Wallis BD, Buratti BJ, Baines KH, et al. Self-gravity wake structures in Saturn's A ring revealed by Cassini VIMS. *Astron J* 2007;133:2624–9.
- [22] Colwell JE, Esposito LW, Sremčević M. Self-gravity wakes in Saturn's A ring measured by stellar occultations from Cassini. *Geophys Res Lett* 2006;33:L07201.
- [23] Colwell JE, Esposito LW, Sremčević M, Stewart GR, McClintock WE. Self-gravity wakes and radial structure of Saturn's B ring. *Icarus* 2007;190:127–44.
- [24] Lyot B. Recherche sur la polarisation de la lumière des planètes et de quelques substances terrestres. *Ann Obs Meudon VIII* 1929;8:1–161.
- [25] Franklin FA, Cook AF. Optical properties of Saturn's rings. II. Two-color phase curves of the two bright rings. *Astron J* 1965;70:704–20.
- [26] Mishchenko MI, Dlugach JM. Can weak localization of photons explain the opposition effect of Saturn's rings. *Mon Not R Astron Soc* 1992;254:15P–8P.
- [27] Mishchenko MI. On the nature of the polarization opposition effect exhibited by Saturn's rings. *Astrophys J* 1993;411:351–61.
- [28] Dollfus A. Saturn's rings: optical reflectance polarimetry. *Icarus* 1996;124:237–61.
- [29] Rosenbush VK, Avramchuk VV, Rosenbush AE, Mishchenko MI. Polarization properties of the Galilean satellites of Jupiter: observations and preliminary analysis. *Astrophys J* 1997;487:402–14.
- [30] Doyle LR, Grün E. Radiative transfer modeling constraints on the size of the spoke particles in Saturn's rings. *Icarus* 1990;85:168–90.
- [31] McGhee CA, French RG, Dones L, Cuzzi JN, Salo HJ, Danos R. HST observations of spokes in Saturn's B ring. *Icarus* 2005;173:508–21.
- [32] Nicholson PD, Hedman MM, Clark RN, Showalter MR, Cruikshank DP, Cuzzi JN, et al. A close look at Saturn's rings with Cassini VIMS. *Icarus* 2008;193:182–212.
- [33] Cuzzi JN, Estrada PR. Compositional evolution of Saturn's rings due to meteoroid bombardment. *Icarus* 1998;132:1–35.
- [34] Poulet F, Cruikshank DP, Cuzzi JN, Roush TL, French RG. Compositions of Saturn's rings A, B, and C from high resolution near-infrared spectroscopic observations. *Astron Astrophys* 2003;412:305–16.
- [35] Esposito LW. Planetary rings. *Rep Progr Phys* 2002;65:1741–83.
- [36] Cuzzi JN, Colwell JE, Esposito LW, Porco CC, Murray CD, Nicholson PD, et al. Saturn's rings: pre-Cassini status and mission goals. *Space Sci Rev* 2002;104:209–51.